The excitation and detection of a leaky surface electromagnetic wave on a high-index dielectric grating in a prism-coupler geometry

I. Simonsen[a)]

Department of Physics, NTNU Norwegian University of Science and Technology, NO-7491 Trondheim, Norway Surface du Verre et Interfaces, UMR 125 CNRS/Saint-Gobain, F-93303 Aubervilliers, France

A. A. Maradudin

Department of Physics and Astronomy, University of California, Irvine, California 92697, USA
(Submitted August 2, 2016)
Fiz. Nizk. Temp. **43**, 193–199 (January 2017)

A periodically corrugated interface between vacuum and a high-index dielectric medium supports a *p*-polarized leaky surface electromagnetic wave whose sagittal plane is perpendicular to the generators of the interface. This wave is bound to the surface in the vacuum region, but radiates into the high-index dielectric medium. We study the excitation of this wave by *p*-polarized light incident from a prism on whose planar base the highindex dielectric medium in the form of a film is bonded. The unilluminated surface of the film is periodically corrugated, and is in contact with vacuum. Peaks and dips in the dependence of several low-order diffraction efficiencies on the angle of incidence (Wood anomalies) are the signatures of the excitation of the surface wave. *Published by AIP Publishing*. [http://dx.doi.org/10.1063/1.4974194]

I. INTRODUCTION

In recent work[1] the present authors have shown theoretically that a periodically corrugated interface between a high index dielectric medium and vacuum supports a *p*-polarized leaky surface electromagnetic wave. This wave is bound to the surface in the vacuum and radiates into the high-index dielectric medium. In this study[1] it was also shown that this wave can be excited by a plane wave incident on the periodic vacuum-dielectric interface from the high-index medium, and observed through the Wood anomalies observed in the dependence of the reflectivity and other low-order diffraction efficiencies on the polar angle of incidence.

Although the calculation of the diffraction efficiencies with the assumption of incidence from a high-index dielectric medium sufficed for establishing a proof of concept for the existence of the leaky surface wave, it seemed that a more conventional approach to its observation would be useful to have. In this paper we provide such an approach. We will study the excitation of the leaky surface electromagnetic wave by the use of a prism-coupler geometry, known as the Kretschmann–Raether geometry.[2] In this geometry a film of the high-index dielectric material is bonded to its planar interface with the prism through which it is illuminated. The periodically corrugated surface of this film is in contact with vacuum. The excitation of the leaky surface wave propagating along the corrugated film-vacuum interface is revealed by the presence of peaks and dips in the dependence of the reflectivity and other low-order diffraction efficiencies on the angle of incidence. The calculation of the amplitudes of the diffracted and refracted beams will be carried out through the solution of the reduced Rayleigh equations they satisfy. Because the dispersion curve for the surface wave supported by this structure differs slightly from what it is for a wave propagating along a high-index grating in contact with vacuum, we also calculate this dispersion curve by the solution of the homogeneous version of the reduced Rayleigh equation for this geometry to help in interpreting the diffraction results.

II. THEORETICAL FORMULATION

The system we study consists of a dielectric material whose dielectric constant is ε_1 in the region $x_3 > 0$; a dielectric medium whose dielectric constant is ε_2 in the region $-H + \zeta(x_1) < x_3 < 0$; and a dielectric material whose dielectric constant is ε_3 in the region $x_3 < -H + \zeta(x_1)$ (Fig. 1). We assume that ε_1, ε_2 and ε_3 are all real, positive, and frequency independent. In the numerical calculations that will be carried out in this paper, ε_1 will be assumed to be the dielectric constant of the prism, ε_2 will be the dielectric constant of the high-index dielectric medium, and ε_3 will be the dielectric constant of vacuum. The interface profile function $\zeta(x_1)$ is assumed to be a single-valued, differentiable, and periodic function of x_1 with period a, $\zeta(x_1 + a) = \zeta(x_1)$. We consider

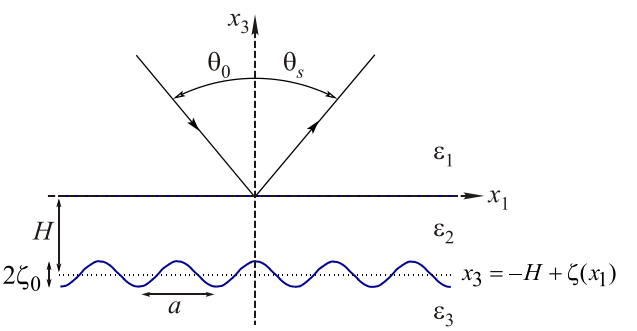

FIG. 1. A depiction of the system studied in this paper.

the case of a p-polarized electromagnetic field in this system, whose plane of incidence, and scattering, is the x_1x_3 plane.

We consider both the diffraction in reflection and transmission of a plane wave of frequency ω incident from the region $x_3 > 0$ on the interface $x_3 = 0$. The dispersion relation for the surface electromagnetic wave supported by this structure can be extracted from the equation for the diffraction amplitudes, while the degree to which the diffracted and refracted fields satisfy unitarity is an indication of the accuracy of our numerical work.

The single nonzero component of the magnetic field in each of the three regions of our system can be written as

$$H_2^{(1)}(x_1,x_3|\omega) = \exp\left[ikx_1 - i\alpha_1(k,\omega)x_3\right] + \sum_{n=-\infty}^{\infty} R_n(k,\omega) \times \exp\left[ik_n x_1 + i\alpha_1(k_n,\omega)x_3\right] \tag{1a}$$

in the region $x_3 > 0$, as

$$H_2^{(2)}(x_1,x_3|\omega) = \sum_{n=-\infty}^{\infty} \exp(ik_n x_1) \times \{A_n(k,\omega)\exp[i\alpha_2(k_n,\omega)x_3] + B_n(k,\omega)\exp[-i\alpha_2(k_n,\omega)x_3]\} \tag{1b}$$

in the region $-H + \zeta(x_1) < x_3 < 0$, and as

$$H_2^{(3)}(x_1,x_3|\omega) = \sum_{n=-\infty}^{\infty} T_n(k,\omega)\exp\left[ik_n x_1 - i\alpha_3(k_n,\omega)x_3\right] \tag{1c}$$

in the region $x_3 < -H + \zeta(x_1)$. A harmonic time dependence $\exp(-i\omega t)$ has been assumed in writing these equations, but it has not been indicated explicitly. In Eq. (1) $k_n = k + 2\pi n/a$, and $\alpha_j\ (k,\ \omega) = [\varepsilon_j\ (\omega/c)^2\ -\ k^2]^{1/2}$ $(j = 1,\ 2,\ 3)$. The way in which the branch cut defining the square roots in these expressions will be described below. The reduced Rayleigh equation for the diffraction amplitudes $\{R_n\ (k,\ \omega)\}$ is[3]

$$\sum_{n=-\infty}^{\infty} [M^{(+)}(k_m|k_n)I_{m-n}(\alpha_3(k_m,\omega) - \alpha_2(k_n,\omega)) + M^{(-)}(k_m|k_n)I_{m-n}(\alpha_3(k_m,\omega) + \alpha_2(k_n,\omega))]R_n(k,\omega) = N^{(+)}(k_m|k)I_m(\alpha_3(k_m,\omega) - \alpha_2(k,\omega)) + N^{(-)}(k_m|k) \times I_m(\alpha_3(k_m,\omega) + \alpha_2(k,\omega)), \quad m = 0, \pm1, \pm2, \ldots, \tag{2}$$

where

$$M^{(\pm)}(k_m|k_n) = \frac{\alpha_3(k_m,\omega)\alpha_2(k_n,\omega) \pm k_m k_n}{\alpha_3(k_m,\omega) \mp \alpha_2(k_n,\omega)} \frac{\exp[\mp i\alpha_2(k_n,\omega)H]}{\alpha_2(k_n,\omega)} \times [\varepsilon_2\alpha_1(k_n,\omega) \pm \varepsilon_1\alpha_2(k_n,\omega)], \tag{3a}$$

$$N^{(\pm)}(k_m|k) = \frac{\alpha_3(k_m,\omega)\alpha_2(k,\omega) \pm k_m k}{\alpha_3(k_m,\omega) \mp \alpha_2(k,\omega)} \frac{\exp[\mp i\alpha_2(k,\omega)H]}{\alpha_2(k,\omega)} \times [\varepsilon_2\alpha_1(k,\omega) \mp \varepsilon_1\alpha_2(k,\omega)]. \tag{3b}$$

In writing Eq. (2) we have introduced the function

$$I_m(\gamma) = \frac{1}{a}\int_{-\frac{a}{2}}^{\frac{a}{2}} dx_1 \exp\left(-i\frac{2\pi m}{a}x_1\right)\exp\left(-i\gamma\zeta(x_1)\right). \tag{4}$$

The diffraction efficiency of the mth scattered beam is the fraction of the total time-averaged incident flux that is diffracted into this beam. It is given by

$$e_m^{(s)} = \frac{\alpha_1(k_m,\omega)}{\alpha_1(k,\omega)}|R_m(k,\omega)|^2. \tag{5}$$

The reflectivity is given by $e_0^{(s)}$.

The reduced Rayleigh equation for the transmission amplitudes $\{T_n\ (k,\ \omega)\}$ is[4]

$$\sum_{n=-\infty}^{\infty} \left[I_{m-n}(\alpha_2(k_m,\omega) + \alpha_3(k_n,\omega))\hat{M}^{(+)}(k_m|k_n) + I_{m-n}(-\alpha_2(k_m,\omega) + \alpha_3(k_n,\omega))\hat{M}^{(-)}(k_m|k_n)\right]T_n(k,\omega) = \delta_{m0}\frac{4\varepsilon_2\varepsilon_3}{\varepsilon_2 - \varepsilon_3}\alpha_1(k,\omega)\alpha_2(k,\omega), \quad m = 0, \pm1, \pm2, \ldots, \tag{6}$$

where

$$\hat{M}^{(\pm)}(k_m|k_n) + [\varepsilon_2\alpha_1(k_m,\omega) \mp \varepsilon_1\alpha_2(k_m,\omega)] \times \frac{\pm k_m k_n - \alpha_2(k_m,\omega)\alpha_3(k_n,\omega)}{\pm\alpha_2(k_m,\omega) + \alpha_3(k_n,\omega)} \times \exp\left\{i[\pm\alpha_2(k_m,\omega) + \alpha_3(k_n,\omega)]H\right\}. \tag{7}$$

The transmission efficiency of the mth transmitted beam is

$$e_m^{(t)} = \frac{\varepsilon_1}{\varepsilon_3}\frac{\alpha_3(k_m,\omega)}{\alpha_1(k,\omega)}|T_m(k,\omega)|^2. \tag{8}$$

For the lossless system we are studying the conservation of energy in the scattering/transmission processes (unitarity) is expressed by

$$\sum_m{}' e_m^{(s)} + \sum_m{}' e_m^{(t)} = 1, \tag{9}$$

where the prime on each sum indicates that it is taken over only the open channels, i.e., those for which $\alpha_1(k_m,\omega)$ and $\alpha_3(k_m,\omega)$ are real.

III. THE DISPERSION RELATION FOR LEAKY SURFACE ELECTROMAGNETIC WAVES

We obtain the dispersion relation for the surface electromagnetic wave supported by this structure by removing the incident field from the right-hand side of Eq. (1a). This is equivalent to deleting the inhomogeneous term from Eq. (2). In this way we obtain the homogeneous system of equations for the amplitudes $\{R_n\ (k,\omega)\}$ of the diffracted beams,

$$\sum_{n=-\infty}^{\infty} M_{mn}(k,\omega)R_n(k,\omega) = 0, \quad m = 0, \pm1, \pm2, \ldots, \tag{10a}$$

where

$$M_{mn}(k,\omega) = M^{(+)}(k_m|k_n)I_{m-n}(\alpha_3(k_m,\omega) - \alpha_2(k_n,\omega)) + M^{(-)}(k_m|k_n)I_{m-n}(\alpha_3(k_m,\omega) + \alpha_2(k_n,\omega)). \tag{10b}$$

The solvability condition for this system of equations, namely the vanishing of the determinant of the matrix of coefficients in Eq. (10),

$$D(k,\omega) = \det[\mathbf{M}(k,\omega) = 0], \tag{11}$$

is the dispersion relation we seek.

The solutions $\omega(k)$ of Eq. (11) are even functions of k, $\omega(-k) = \omega(k)$, and are periodic functions of k with a period $2\pi/a$, $\omega(k + 2\pi/a) = \omega(k)$. Therefore, all of the solutions of Eq. (11) are obtained if we restrict k to the interval $0 \leq k \leq \pi/a$. This is called the reduced zone scheme, and we adopt it here. The resulting dispersion curve consists of an infinite number of branches of increasing frequency.

There are three light lines in the system we consider, defined by the dispersion curves $\omega = kc/\sqrt{\varepsilon_j}$, with $j = 1$, 2, 3. In the geometry we are assuming, where $\varepsilon_2 > \varepsilon_1 > \varepsilon_3$, we must have $k < \sqrt{\varepsilon_1}(\omega/c)$ for propagating incident and diffracted fields in the prism; $k < \sqrt{\varepsilon_2}(\omega/c)$ to have a radiative field in the high-index dielectric film; and $k < \sqrt{\varepsilon_3}(\omega/c)$ to have a field decaying exponentially into the vacuum with increasing distance from the corrugated surface of the high-index dielectric. Therefore, it is in the region of the (ω, k)-plane defined by $\sqrt{\varepsilon_3}(\omega/c) < k < \sqrt{\varepsilon_1}(\omega/c)$ that solutions of Eq. (11) will be sought, with $0 \leq k \leq \pi/a$. In this region the frequency of the surface wave is complex, $\omega(k) = \omega_R(k) - i\omega_I(k)$, where $\omega_R(k)$ and $\omega_I(k)$ are real and positive. The negative sign of the imaginary part of the frequency reflects the decrease of the amplitude of the wave in time as it propagates due to its radiation into the high-index film.

To obtain solutions of Eq. (11) that possess these properties the branch cut that defines the square root in the definition of $\alpha_j(k_m,\omega)$ must be chosen properly. It has been shown in Ref. 6 that if the branch cut is taken along the negative imaginary axis the leaky surface wave will have the desired properties.

The method by which Eq. (11) is solved numerically is described in detail in Ref. 6, to which we refer the reader.

IV. RESULTS AND DISCUSSIONS

To illustrate the preceding results we present plots of the dispersion curve for the leaky surface electromagnetic wave, and of the dependence of the reflectivity/transmissivity and other diffraction efficiencies on the angle of incidence $\theta 0$, when the surface profile function has the cosine form

$$\zeta(x_1) = \zeta_0 \cos\left(\frac{2\pi x_1}{a}\right), \tag{12}$$

with $\zeta_0 \geq 0$ and $a > 0$. For this profile function the function $I_m(\gamma)$, defined by Eq. (4), is given by

$$I_m(\gamma) = (-i)^m J_m(\gamma\zeta_0), \tag{13}$$

where $J_m(z)$ is a Bessel function of the first kind of order m.

A. Dispersion curves

In Fig. 2(a) we present the plot of $\omega_R(k)$ as a function of k for the case where $\varepsilon_1 = 2.25$, $\varepsilon_2 = 15$, and $\varepsilon_3 = 1$. The surface profile function is given by Eq. (12) with $\zeta_0/a = 0.10$ and the mean width of the high-index film $H/a = 0.20$. These parameter values will be used in all of the calculations reported in this paper. In obtaining this result, the infinite-dimensional matrix $\mathbf{M}(k,\omega)$ in Eq. (11) was replaced by a $(2N + 1) \times (2N + 1)$ matrix by restricting the indices m and n that appear in Eq. (10b) to the values $-N, -N+1, \ldots, N-1, N$. In the present calculations N was given the value 15; increasing N above this value was found to produce results

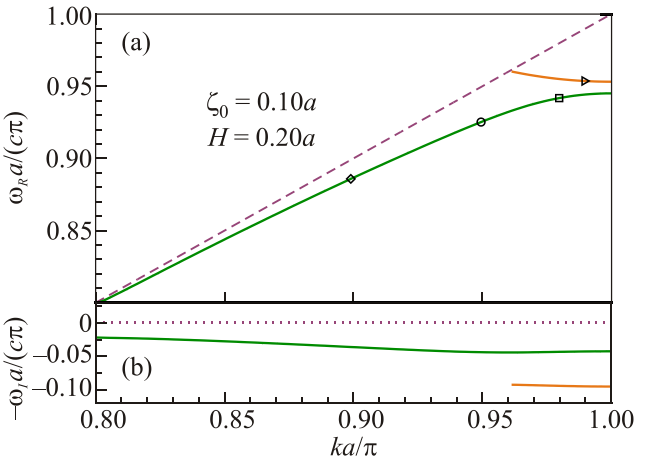

FIG. 2. The (a) real part $\omega_R(k)$ and (b) the imaginary part $\omega_I(k)$ of the complex frequency $\omega(k) = \omega_R(k) - i\omega_I(k)$ of the leaky surface electromagnetic wave supported by the structure depicted in Fig. 1. The values of the parameters defining this structure are $\varepsilon_1 = 2.25$, $\varepsilon_2 = 15$, and $\varepsilon_1 = 1$. The surface profile function is $\zeta(x_1) = \zeta_0 \cos(2\pi x_1/a)$ [Eq. (12)], with $\zeta_0/a = 0.10$ and $H/a = 0.20$. A 31×31 matrix system (i.e., $N = 15$) was used to obtain these results. The vacuum light line is indicated by a dashed line in panel (a). The open symbols in panel (a) indicate some frequencies that are discussed in the main text.

that were essentially indistinguishable from those obtained using $N = 15$ but at the cost of longer calculation times.

We see from Fig. 2(a) that in the region of wavenumbers $\sqrt{\varepsilon_3}(\omega/c) < k < \sqrt{\varepsilon_1}(\omega/c)$ in which the leaky surface wave is expected to exist, $\omega_R(k)$ has two branches, a low frequency branch that approaches the vacuum light line as k decreases, and a high frequency branch separated from it by a gap at the Brillouin zone boundary $k = \pi/a$, that ends where it intersects the vacuum light line.

In Fig. 2(b) we present the $\omega_I(k)$ corresponding to each of the two branches of $\omega_R(k)$ plotted in Fig. 2(a). We see from this figure that the ratio ω_I/ω_R is of the order -0.03 for the lower frequency branch, while it is of the order -0.10 for the high frequency branch. This difference will manifest itself in the diffraction results to which we now turn.

B. Rayleigh and Wood anomalies

A way to excite an electromagnetic surface wave supported by a periodically corrugated surface is to diffract light from it and examine the dependence of the diffraction efficiencies on the angle of incidence for signatures of this excitation in the form of anomalies in these dependencies. Two types of anomalies are observed in these dependencies. The first kind of anomaly occurs at angles of incidence for a fixed wavelength of the incident light at which a diffraction order appears or disappears (in reflection or transmission). The values of these angles depend only on the wavelength of the incident light and the period a of the corrugated surface. They are called Rayleigh anomalies after the scientist who explained their origin.[6] The second type of anomaly occurs at angles of incidence at which the tangential component of the wave vector of the incident light, supplemented by a positive or negative multiple of $2\pi/a$, matches the wavenumber of the surface wave supported at the frequency of the incident light. Although this explanation of the origin of these anomalies was first given by Fano,[7] they are called Wood anomalies after Wood[8,9] who discovered them and the

Rayleigh anomalies. Thus, it is the Wood anomalies that are the signature of the excitation of surface waves.

For the system we study the values of θ_0 at which the Rayleigh anomalies are expected to occur are given by

$$\sin\theta_0^{(m)} = \pm 1 - \frac{2m}{\sqrt{\varepsilon_1}}\left(\frac{\omega}{c}\frac{a}{\pi}\right)^{-1} \tag{14a}$$

in reflection, and

$$\sin\theta_0^{(m)} = \pm\sqrt{\frac{\varepsilon_3}{\varepsilon_1}} - \frac{2m}{\sqrt{\varepsilon_1}}\left(\frac{\omega}{c}\frac{a}{\pi}\right)^{-1} \tag{14b}$$

in transmission. In both of these expressions m is a positive or negative integer ($m \in \mathbb{N}$), ω is the frequency of the incident light, and a is the period of the grating.

The values of θ_0 at which Wood anomalies are expected to occur are given by

$$\sin\theta_0^{(m)} = \frac{1}{\sqrt{\varepsilon_1}}\left(\frac{\omega}{c}\frac{a}{\pi}\right)^{-1}\left[\pm k_{sw}(\omega)\frac{a}{\pi} - 2m\right], \tag{15}$$

where $k_{sw}(\omega)$ is the wavenumber of the leaky surface electromagnetic wave, the real part of whose frequency equals that of the incident light. The value of $k_{sw}(\omega)$ is restricted to the interval $0 \le k_{sw}(\omega) \le \pi/a$. In obtaining Eqs. (14) and (15) we have used the relation between k and θ_0 given by $k = \sqrt{\varepsilon_1}\,(\omega/c)\sin\theta_0$.

C. Diffraction efficiencies

In Fig. 3(a) we plot the diffraction efficiencies in reflection $e_m^{(s)}$, while in Fig. 3(b) we plot them in transmission $e_m^{(t)}$, as functions of the angle of incidence in the prism θ_0. These results were obtained under the assumption that the frequency of the incident light is $\omega a/c\pi = 0.9252$ which is indicated by the circle on the dispersion curve in Fig. 2(a). Only results for positive values of θ_0 are presented, because a feature presented at a positive value of θ_0 with a given sign of m will occur at $-\theta_0$ with the opposite sign of m. For the parameters assumed in obtaining the results presented in Fig. 3 only three non-zero (open) diffraction channels ($m = 0, \pm 1$) exist in both reflection and transmission, and three Rayleigh anomalies are predicted. The first of these anomalies is due to reflection and is, according to Eq. (14a), expected to occur at an angle of incidence $\theta_0 = \pm 26.18°$. The two remaining Rayleigh anomalies are due to transmission and are predicted by Eq. (14b) to occur at $\theta_0 = \pm 41.81°$ and $\pm 50.76°$. It is interesting to note that the angular position of the first of these Rayleigh anomalies for transmission is identical to the critical angle for total internal reflection for the corresponding planar interface system ($\zeta_0 = 0$), $\theta_c = \pm\arcsin(\sqrt{\varepsilon_3/\varepsilon_1})$; this is readily seen from Eq. (14b) with $m = 0$ from which it also follows that the position of this Rayleigh anomaly should be independent of the frequency of the incident light (see Figs. 3–6). Moreover, for the system studied in Fig. 1 two Wood anomalies are expected to occur at the angular positions $\theta_0 = \pm 43.17°$ and $\pm 46.23°$ predicted by Eq. (15). In Fig. 3, and in the remaining figures, the angular positions of the Rayleigh anomalies are indicated by vertical dash-dotted lines, while the positions of the Wood anomalies are indicated by vertical dashed lines.

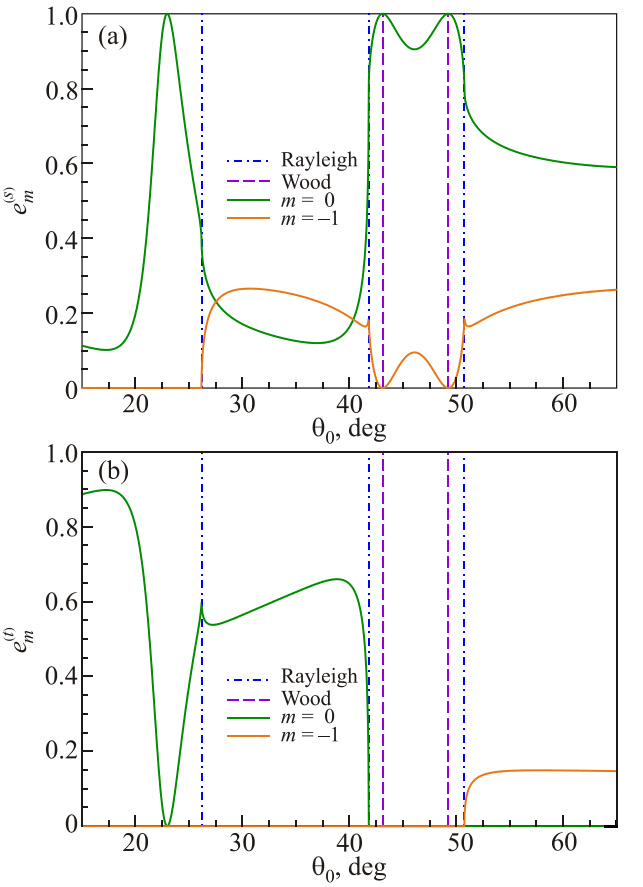

FIG. 3. The diffraction efficiencies in (a) reflection $e_m^{(s)}$ and (b) transmission $e_m^{(t)}$ as functions of the angle of incidence θ_0. The vacuum wavelength of the incident light is $\lambda/a = 2.1617$ [$\omega_R a/c\pi = 0.9252$], and is indicated by the circle on the dispersion curve in Fig. 2(a) at $ka/\pi = 0.9495$. Rayleigh anomalies are expected at angles of incidence $\theta_0^R = \pm 26.18°$, $\pm 41.81°$ and $\pm 50.76°$ (dash-dotted lines) [Eq. (14)]. Wood anomalies are predicted from Eq. (15) to occur at angles of incidence $\theta_0^W = \pm 43.17°$ and $\pm 46.23°$ (dashed lines). The value $N = 15$ was assumed in solving the reduced Rayleigh equations for reflection and transmission [Eqs. (2) and (6)].

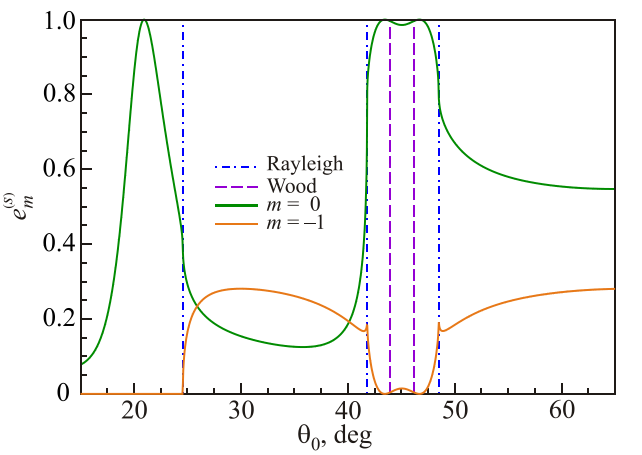

FIG. 4. The diffraction efficiencies in reflection $e_m^{(s)}$ as functions of the angle of incidence θ_0. The vacuum wavelength of the incident light is $\lambda/a = 2.1236$ [$\omega_R a/c\pi = 0.9418$], and is indicated by the square on the dispersion curve in Fig. 2(a) at $ka/\pi = 0.9798$. Rayleigh anomalies are expected at angles of incidence $\theta_0^R = \pm 24.57°$, $\pm 41.81°$ and $\pm 48.51°$ (dash-dotted lines). Wood anomalies are predicted from Eq. (15) to occur at angles of incidence $\theta_0^W = \pm 43.91°$ and $\pm 46.23°$ (dashed lines).

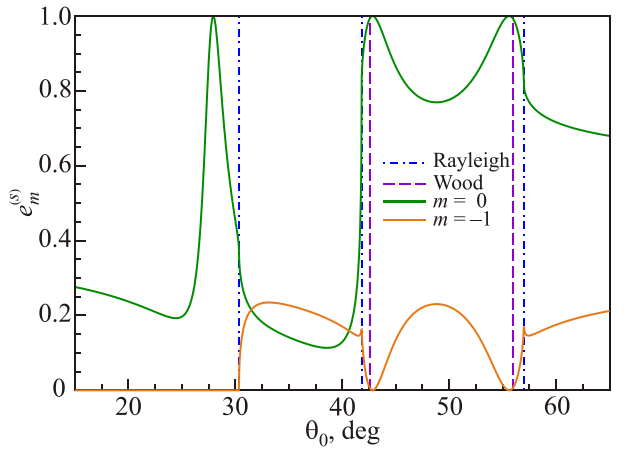

FIG. 5. The diffraction efficiencies in reflection $e_m^{(s)}$ as functions of the angle of incidence θ_0. The vacuum wavelength of the incident light is $\lambda/a = 2.2578$ [$\omega_R a/c\pi = 0.8858$], and is indicated by the diamond on the dispersion curve in Fig. 2(a) at $ka/\pi = 0.8990$. Rayleigh anomalies are expected for angles of incidence $\theta_0^R = \pm 30.34°$, $\pm 41.81°$ and $\pm 56.98°$ (dash-dotted lines). Wood anomalies are predicted from Eq. (15) to occur at angles of incidence $\theta_0^W = \pm 42.58°$ and $\pm 55.96°$ (dashed lines).

We now turn to the dependencies of the diffraction efficiencies on θ_0, and our main focus will be on their behavior around the Rayleigh and Wood anomalies. From the results presented in Fig. 3 we observe an excellent agreement between the positions of the Rayleigh anomalies seen in the simulated diffracted efficiency curves for reflection and transmission and the angles of incidence predicted by Eq. (14). The results in Fig. 3(a) show that the Rayleigh anomalies express themselves as vertical tangents in the reflectivity and as a cutoff and as sharp peaks in the diffraction efficiency $e_{-1}^{(s)}$. The Wood anomalies appear in the reflected efficiencies and their angular positions are well predicted by Eq. (15). These anomalies express themselves as peaks in the reflectivity and dips in the diffraction efficiency $e_{-1}^{(s)}$ [Fig. 3(a)].

In transmission [Fig. 3(b)] the vertical tangent in the reflectivity at $\theta_0 = 26.18°$, indicating a Rayleigh anomaly, is transformed into a sharp peak at the same angle. The two

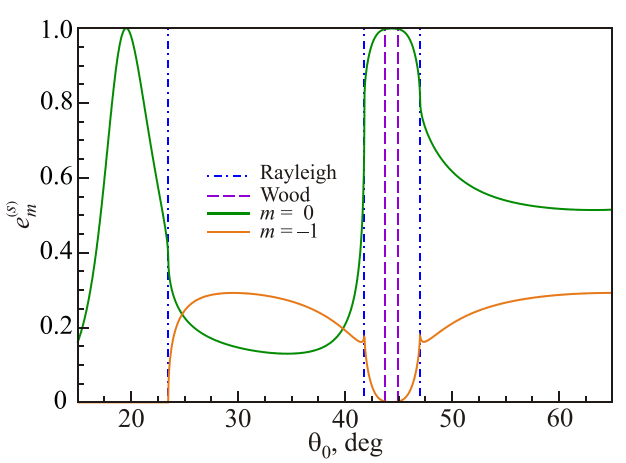

FIG. 6. The diffraction efficiencies in reflection $e_m^{(s)}$ as functions of the angle of incidence θ_0. The vacuum wavelength of the incident light is $\lambda/a = 2.0972$ [$\omega_R a/c\pi = 0.9536$], and is indicated by the triangle on the dispersion curve in Fig. 2(a) at $ka/\pi = 0.9896$. Rayleigh anomalies are expected for angles of incidence $\theta_0^R = \pm 23.46°$, $\pm 41.81°$ and $\pm 47.01°$ (dash-dotted lines). Wood anomalies are predicted from Eq. (15) to occur at angles of incidence $\theta_0^W = \pm 43.77°$ and $\pm 44.94°$ (dashed lines).

sharp peaks in the reflectivity at $\theta_0 = 41.81°$ and $50.76°$ mark the disappearance of the transmissivity and the appearance of the $e_{-1}^{(t)}$ efficiency, respectively. No Wood anomalies occur in transmission. One observes from Fig. 3(b) that there is actually no transmitted intensity for angles of incidence in the interval $41.81° < |\theta_0| < 50.76°$, and, therefore, the transmitted intensity is also zero at the angular positions where Wood anomalies are expected. The reason for this behavior is that no diffraction channels in transmission are open over this range of angles of incidence, as can be readily demonstrated.

In the calculations of the diffraction efficiencies that appear in Fig. 3 as well as in the remaining figures of this paper, the branch cut defining the square root in $\alpha_j(k,\omega)$ $(j = 1,2,3)$ was taken along the negative real axis, and ω and k were real.

It should be remarked that for the calculations that produced the results presented in Fig. 3, the energy conservation condition (9) was found to be satisfied within an error no greater than 2×10^{-4} for any angle of incidence θ_0 in the interval from $-90°$ to $90°$. This testifies to the accuracy of the simulation approach that we use. The energy conservation was also checked explicitly for all the remaining diffraction calculations that we will present in this paper, even if no further results for diffraction efficiencies in transmission will be given. In all the calculations of diffraction efficiencies that we report in this paper the error in the satisfaction of the energy conservation, Eq. (9), was of the order 10^{-4}, or less.

In Fig. 4 we present the diffraction efficiencies in reflection $(e_m^{(s)})$ as functions of θ_0, corresponding to the point indicated by the square on the dispersion curve plotted in Fig. 2(a). The Rayleigh anomalies appear as vertical tangents in the reflectivity, at precisely the angles predicted by Eq. (14), while the Wood anomalies appear as a pair of closely spaced peaks at the angles predicted by Eq. (15). In results for $e_{-1}^{(s)}$ the Rayleigh anomalies appear as an angle at which the $m = -1$ diffraction order appears, $\theta_0 = 24.57°$, and as sharp peaks (arising from transmission) at $\theta_0 = 41.81°$ and $45.51°$. The Wood anomalies occur as two closely spaced minima in this diffractive order.

In our next example, the frequency of the incident light is $\omega a/c\pi = 0.8858$, and it is indicated by the diamond in Fig. 2(a). Figure 5 presents the angle of incidence dependence of the diffraction efficiencies in reflection for this frequency. The Rayleigh and Wood anomalies in this case have the same forms as they do in Figs. 3 and 4, except that the angular positions of each type of anomaly are now widely separated, while the separations between the Rayleigh and Wood anomalies are smaller.

The results displayed in Figs. 3–5 have all assumed that the frequency of the incident light corresponds to points on the lower branch of dispersion curve in Fig. 2(a). As our final result we present in Fig. 6 the diffraction efficiencies in reflection as functions of the angle of incidence θ_0, assuming a frequency of the incident light that corresponds to the point indicated by the triangle in Fig. 2(a). The forms of the Rayleigh anomalies in the angular dependencies of the reflectivity and $e_{-1}^{(s)}$ are the same as in Figs. 3–5, and appear where predicted by Eq. (14). However, the Wood anomalies in the reflectivity and $e_{-1}^{(s)}$ are now no longer visible as peaks and dips, respectively. This is because they are now closely

separated and each peak is broad, because from Fig. 2(b) we see that the corresponding mode is strongly damped.

Of the cases considered in this paper, the two that offers the best opportunities for exciting and detecting the leaky surface electromagnetic wave on a high-index dielectric grating are the those whose results are presented in Figs. 3 and 5.

V. CONCLUSIONS

In this paper we have shown that a leaky surface electromagnetic wave on a periodically corrugated high-index dielectric surface of the kind predicted in Ref. 1, can be excited and observed in a prism-coupler geometry (Kretschmann–Raether geometry). As is usual in the theoretical and experimental determination of the dispersion curve by this method, the dispersion curve obtained differs slightly from the curve predicted theoretically for a singleinterface structure,[10] but it is the curve that is actually measured. We hope that these results will encourage experimental efforts to detect this mode.

We dedicate this paper to the memory of Ilya Mikhailovich Lifshitz on the occasion of his 100th birthday. He was a brilliant physicist and a great human being, whom one of us (A.A.M.) had the pleasure of knowing.

The research of I.S. was supported in part by The Research Council of Norway Contract No. 216699.

[a)]Email: ingve.simonsen@gmail.com

[1]A. A. Maradudin, I. Simonsen, and W. Zierau, Opt. Lett. **41**, 2229 (2016).
[2]E. Kretschmann and H. Raether, Z. Naturforsch. A **23**, 2135 (1968).
[3]G. Berginc and A. A. Maradudin, in *Optical Thin Films and Coatings*, edited by A. Piegari and F. Flory (Woodhead Publishing, Oxford, 2013), p. 177. To obtain Eqs. (2)–(4) one sets $h_1(x) \equiv 0$ in Eq. (6.39) of this reference and assumes $h_2(x)$ is a periodic function of x with a period a.
[4]To obtain Eqs. (6) and (7) one sets $h_1(x) \equiv 0$ in Eq. (6.43) of Ref. 4, and assumes $h_2(x)$ is a periodic function of x with a period a.
[5]A. A. Maradudin, I. Simonsen, J. Polanco, and R. M. Fitzgerald, J. Opt. **18**, 024004 (2016).
[6]Lord Rayleigh, Proc. R. Soc. (London) Ser. A **79**, 399 (1907).
[7]U. Fano, J. Opt. Soc. Am. **31**, 213 (1941).
[8]R. W. Wood, Proc. Phys. Soc., London **18**, 269 (1902).
[9]R. W. Wood, Philos. Mag. **4**, 396 (1902).
[10]E. F. Y. Kou and T. Tamir, Appl. Opt. **27**, 4098 (1988).

This article was published in English in the original Russian journal. Reproduced here with stylistic changes by AIP Publishing.